

CoMFA and CoMSIA studies on a new series of xanthone derivatives against the oral human epidermoid carcinoma (KB) cancer cell line

Ketthip Suphavanich · Phornphimon Maitarad ·
Supa Hannongbua · Pichit Sudta · Sunit Suksamrarn ·
Yuthana Tantirungrotechai · Jumras Limtrakul

Received: 7 March 2008 / Accepted: 2 June 2008 / Published online: 17 September 2008
© Springer-Verlag 2008

Abstract A new series of xanthone derivatives against the oral human epidermoid carcinoma (KB) cancer cell line is examined to determine the relationship between the structural properties and the biological activity of these compounds—the 3-D quantitative structure–activity relationship (3D-QSAR)—using comparative molecular field analysis (CoMFA) and comparative molecular similarity indices analysis (CoMSIA). The best CoMFA and CoMSIA models were obtained using the atom-based alignment of 33 compounds, 22 training compounds and 11 tested compounds, and these give desirable statistics; those for the CoMFA standard model were: $r_{cv}^2 = 0.691$, $r^2 = 0.998$, $S_{press} = 0.178$, $s = 0.014$ and $F = 1080.765$, while CoMSIA combined steric, electrostatic, hydrophobic and hydrogen-bond acceptor fields: $r_{cv}^2 = 0.600$, $r^2 = 0.988$, $S_{press} = 0.206$, $s = 0.034$ and $F = 284.433$. The 3D-QSAR models calculated satisfactory test set activities. The 3D-QSAR contour plots correlated strongly with the experimental data for the binding topology. For this reason,

these results would be beneficial for predicting affinities with the compounds of interest, and they are advantageous for guiding the design and synthesis of new and more effective anticancer agents.

Keywords CoMFA · CoMSIA · Xanthone derivatives · Oral human epidermoid carcinoma (KB) cancer cell line

Introduction

Cancer is a disease that is one of the major causes of death in the world. Cancer is a class of disease or disorder characterized by the uncontrolled division of cells and the ability that these cells have to invade other tissue, either by direct growth into adjacent tissue or by implantation into distant sites by metastasis [1]. Most forms of cancer can be treated and some can be cured, depending on the specific type, location and stage. Chemotherapy is a treatment for cancer that utilizes remedies that can destroy cancer cells [2]. There is a range of drugs which, when introduced into the body, can efficiently reduce the spread or proliferation of cancerous cells. Interactions with vaccinations can make small changes to the pharmacokinetics or pharmacodynamics of a chemotherapy agent that could significantly alter its effectiveness or toxicity [3]. Chemotherapy has developed rapidly, and many new cytotoxic inhibitors have come onto the market in recent years; for example, organotin derivatives [4], urokinase plasminogen activator inhibitors [5], the aurora-kinase family [6], the mammalian target of rapamycin (mTOR) [7] and xanthone derivatives [8].

Recently, there has been a great deal of interest in the potential cytotoxic activity of xanthones (see Fig. 1) [8–15]. Chemically, the xanthone nucleus (or 9H-xanthone-9-one)

K. Suphavanich · Y. Tantirungrotechai (✉)
Department of Chemistry, Faculty of Science,
Mahidol University, Rajthevee, Bangkok 10400, Thailand
e-mail: yt203y@gmail.com

P. Maitarad · S. Hannongbua · J. Limtrakul
Department of Chemistry, Faculty of Science,
Kasetsart University, Bangkok 10900, Thailand

P. Sudta · S. Suksamrarn
Department of Chemistry, Faculty of Science,
Srinakharinwirot University, Bangkok 10110, Thailand

J. Limtrakul
Center of Nanotechnology, Kasetsart University Research
and Development Institute, Kasetsart University,
Bangkok 10900, Thailand

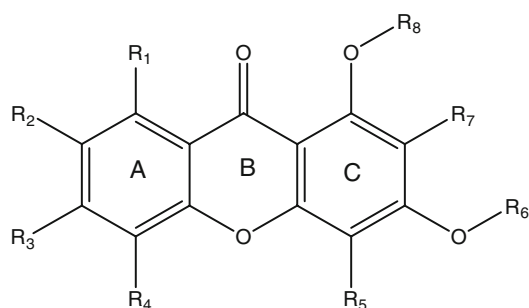


Fig. 1 General structure of xanthone derivatives

comprises an important class of oxygenated heterocycles whose role is well-known in medicinal chemistry [16]. The biological activities of xanthenes are associated with their tricyclic scaffold, but vary depending on the nature and/or position of the different substituents [16–21]. However, there has been no report on the new series of substituted tetraoxygenated xanthenes against the oral human epidermoid carcinoma (KB) cancer cell line.

A 3-D quantitative structure–activity relationship (3D-QSAR) is evaluated using both comparative molecular field analysis (CoMFA) [22] and comparative molecular similarity indices analysis (CoMSIA) [23] in order to study xanthone derivatives against the KB cancer cell line. Such techniques have proven to be the most effective and efficient QSAR techniques and have been successful at generating models for various inhibitors [24–26]. Both CoMFA and CoMSIA methods are eminently suitable for expounding drug–receptor interactions. The steric and electrostatic properties are calculated from Lennard–Jones and Coulombic potential equations in the CoMFA method. In addition, CoMSIA contour plots provide useful advice about electrostatic, steric, hydrophobic, and hydrogen-bonding donor and acceptor properties [27–29].

In this study, both CoMFA and CoMSIA methods are performed on the series of xanthone derivatives; the resulting contour maps illustrate an understanding of the local physicochemical property requirements for ligand binding. Furthermore, the conformation of the spatial orientation of the xanthone derivatives will allow a better understanding that can guide the design of novel anticancer inhibitors.

Results and discussion

CoMFA and CoMSIA statistical results

The CoMFA and CoMSIA techniques were used to derive the 3D-QSAR models for xanthone derivative anticancer inhibitors with pIC_{50} values ranging from 4.70 to 5.68. The

Table 1 Summary of the CoMFA and CoMSIA statistical results

	CoMFA	CoMSIA
Number of components (noc)	6	4
Crossvalidation r_{cv}^2	0.691	0.600
S_{press}	0.178	0.206
Conventional r^2	0.998	0.988
Standard error of estimate (S)	0.014	0.034
F value	1080.765	284.433
Steric	0.527	0.148
Electrostatic	0.473	0.316
Hydrophobic	–	0.324
Hydrogen-bond acceptor	–	0.212
Probe atom	sp^3 C atom	

statistical results of the CoMFA and CoMSIA analyses are summarized in Table 1. The best predictions were obtained with the CoMFA standard model ($r_{cv}^2 = 0.691$, $S_{press} = 0.178$, $\text{noc} = 6$, $r^2 = 0.998$, $s = 0.014$ and F value = 1080.765). In CoMSIA, the steric, electrostatic, hydrophobic and hydrogen-bond acceptor properties are considered. The predictions of the CoMSIA standard model were obtained ($r_{cv}^2 = 0.600$, $S_{press} = 0.206$, $\text{noc} = 4$, $r^2 = 0.988$, $s = 0.034$ and F value = 284.433). The CoMFA results show a higher predictive ability for xanthone derivatives against the KB cell line than the CoMSIA results. The results in Table 1 show the relative contributions of the CoMFA and CoMSIA techniques. Almost equal contributions were observed from steric (54.1%) and electrostatic (45.9%) fields in CoMFA, and the hydrophobic (32.4%) property was the main contributor in CoMSIA. The affinities between the experimental and calculated values of the training set in the CoMFA and CoMSIA models derive from noncrossvalidated analysis, which is plotted in Fig. 2.

Prediction for compounds in the test set

The best CoMFA and CoMSIA models were used to predict the inhibitory activities of the compounds in the test set. A comparison of the experimental data with the calculated inhibitory activities of 11 compounds is reported in Table 2. All compounds are shown in Fig. 3.

CoMFA contour maps

The CoMFA steric and electrostatic fields based on PLS analysis are presented as 3-D contour plots in Fig. 4. Compound 9, α -mangostin, is used as a reference structure in the 3-D plots. The green regions indicate areas where steric bulk enhances biological activity, whereas the yellow contours indicate regions where steric bulk is detrimental

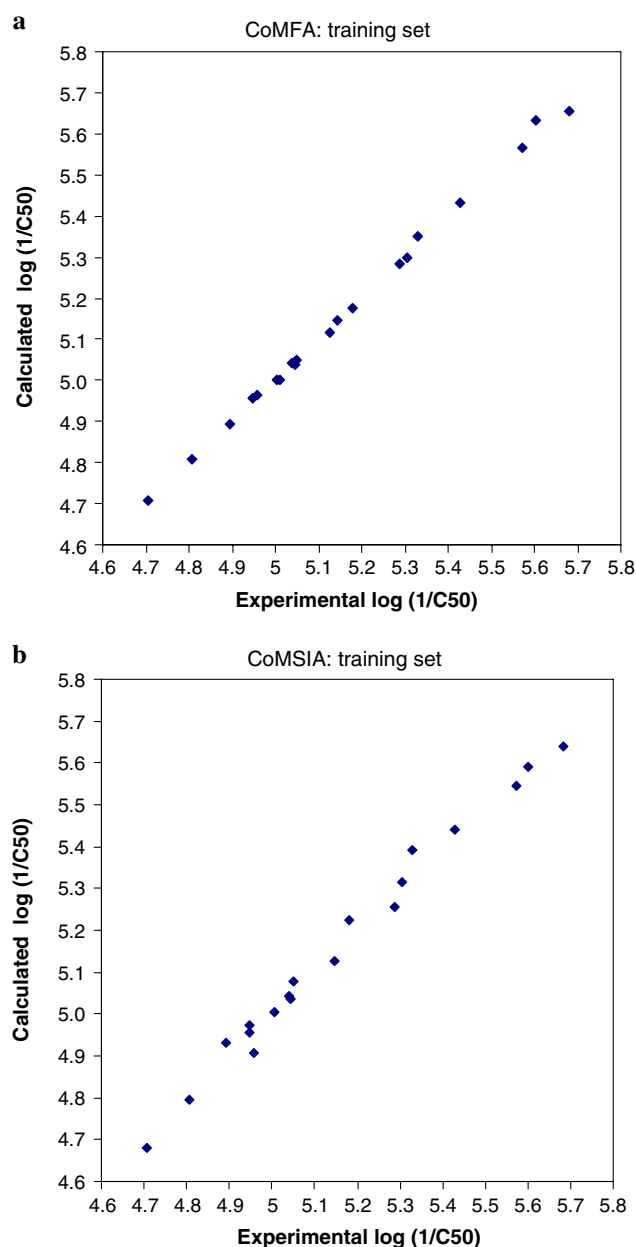


Fig. 2 Plots of experimental versus calculated xanthone derivative affinities obtained from noncrossvalidation of CoMFA (a) and CoMSIA (b)

to biological activity. Blue-colored regions indicate areas where electropositive groups enhance the biological activity, while the red regions represent areas where electronegative groups enhance the biological activity.

The steric contour maps show the green region surrounding the R_1 position. This indicates that bulky substituents are preferred in this area in order to produce higher anticancer activity. Several yellow regions near the R_1 , R_2 , R_3 , R_5 and R_7 positions indicate that the less bulky substituents are preferred for higher activity. The largest yellow region is at the front of R_2 and R_3 . Compound **9** has

Table 2 Experimental and predicted the negative logarithms of IC_{50} KB cell line affinities of the tested xanthone compounds

Compounds	$-\log IC_{50}$		Residual		
	Experimental	Calculated		CoMFA	CoMSIA
		CoMFA	CoMSIA		
1	5.55	5.36	5.34	0.19	0.21
3	4.70	5.20	5.29	−0.50	−0.59
4	4.96	5.32	5.23	−0.36	−0.27
12	5.45	5.30	5.42	0.15	0.03
14	4.88	5.37	5.44	−0.49	−0.56
15	5.67	5.10	5.12	0.57	0.55
20	5.15	5.01	4.94	0.14	0.21
22	5.26	4.91	4.94	0.35	0.32
24	4.80	5.34	5.34	−0.54	−0.54
27	5.33	5.05	5.05	0.28	0.28
31	4.72	5.29	5.20	−0.57	−0.48

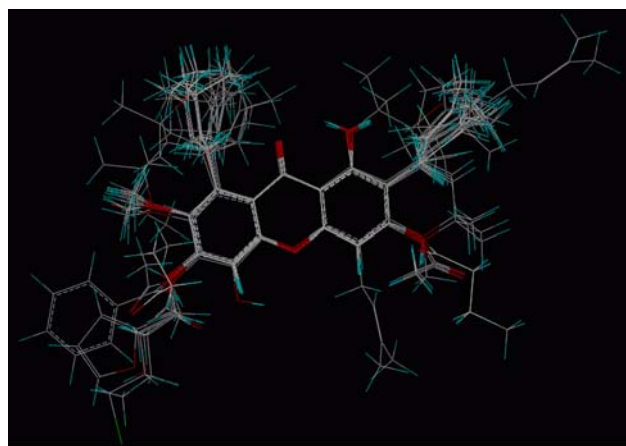
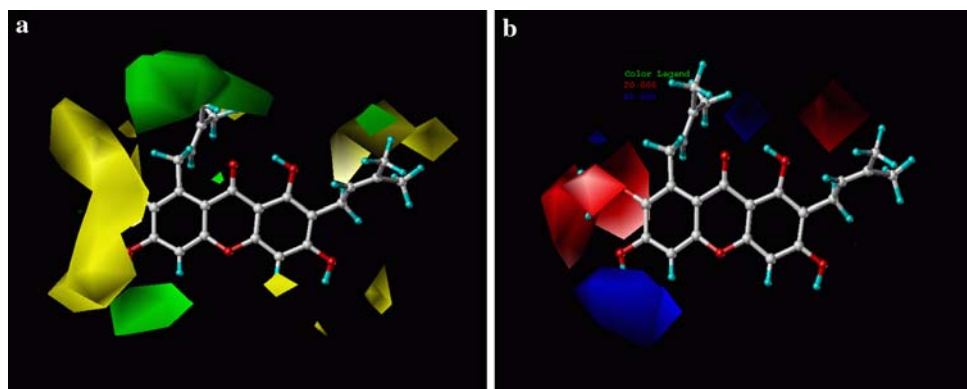


Fig. 3 3-D view of all aligned xanthone derivatives, as prepared by the alignment algorithm

the highest activity and has the bulky substituent (pre) in position R_1 and the less bulky substituents (OH, H) in the R_3 and R_5 positions. This explains why compounds **7** (gartanin) and **16** (3,6,7-tri-*O*-acethylmangostin) have low activities. They have the less bulky substituents in the green regions and the more bulky substituents in the yellow regions. For the electrostatic contour maps, positive charges favored the blue regions which are found between the R_3 and R_4 positions. Negative charges favored the red regions which are found on the left hand side of ring A. These regions illustrate why compounds **19** (6-*O*-benzoylmangostin) and **23** (3-*O*-ethylmangostin) have low activity. That is to say, there is a positively charged hydrogen atom in the red region. Another red region is found above positions R_7 and R_8 . From both the steric and electrostatic contours, it is found that the rear R_1 position might be a bulky substituent and the front of R_2 and R_3 might be a less bulky substituent.

Fig. 4 The two contour maps of the CoMFA ($SD \times \text{coeff}$) model. **a** The steric property; *green areas* indicate regions where bulky groups increase activity; *yellow areas* indicate regions where bulky groups decrease activity. **b** The electrostatic property; *blue areas* indicate regions where positive groups increase activity; *red areas* indicate regions where negative charges increase activity



The reason for the poor activities of compounds **2** (mangostenone D), **19**, **21** (3,6-di-*O*-butanoylmangostin) and **25** (6-*O*-cinnamoylmangostin) is that the R_2 and R_3 positions ought to be a less bulky substituent. This result agrees with compound **16**: this compound has poor activity because the bulky substituent (OAc) is in the yellow region and the positively charged hydrogen atoms in the R_2 positions have a big red region. The difference in activities between compounds **26**, **27**, **29** and **30**, which have the same structures except at the R_3 position, is attributed to the negative charge at the R_3 position. Compound **30** has poor activity owing to the negative charges in the blue region. The R_3 and R_4 positions have a big blue region. The blue region means that the negative charges would decrease the activity. For example, compound **8** (Garcinone E) shows good activity, but because of negative charges in the R_4 position (which is in the blue region) it is less active than compound **9**. Another blue region is above R_8 .

CoMSIA contour maps

The CoMSIA approach is another 3D-QSAR method; it provides different contour plots to CoMFA. It is believed to be less affected by changes in molecular alignment and provides smoother and more interpretable contour maps as a result of employing Gaussian-type distance dependence with molecular similarity indices. The CoMSIA approach was used in this study to consider four different property fields: steric, electrostatic, hydrophobic and hydrogen-bond acceptor. The contour plots obtained from PLS analyses of the CoMSIA model are shown in Fig. 5.

Figure 5a shows the steric contour plots of CoMSIA. The sterically favored green region is found to surround the R_1 position, where a bulky group is well tolerated. A functional (Pre) group or a long chain would be more suitably placed in the green region, corresponding to the CoMFA steric contour maps (Fig. 4a). In contrast, the sterically unfavored yellow regions are found near the R_3 position, between the R_5 and R_6 positions and above the R_7 position, where a large substituent would decrease the

activity. Therefore, substitution with Pre, Me, Ger, and Ac functional groups at these positions results in lower activity than substitution with H.

The electrostatic CoMSIA map (Fig. 5b) indicates red contours in regions where high electron density might cause favorable activity, and blue contours in regions where low electron density might increase the activity. A blue region is also found to surround the R_3 and R_4 positions, as in the CoMFA electrostatic plot (Fig. 4b). Another blue region is depicted between the R_8 position and above ring B.

For the hydrophobic CoMSIA map (Fig. 5c), favorable purple regions are found around the long side chain in the R_1 position, under the R_4 position, and surrounding the R_7 position. This can also explain why compounds **9** and **3**, which have the same group at every position except the R_1 position, have very different activities. Compounds **1**, **5**, **6**, **8**, **9** and **11** have nonpolar groups in the side chain in position R_1 , which indicate hydrophobic regions, the effectiveness of which results in the high activity of these compounds. White, hydrophilic, CoMSIA-favorable regions are found near position R_2 , under position R_3 and between positions R_5 and R_6 . Hence, substitution with the nonpolar groups in the R_3 position of compounds **24** and **31** correlate to the poor activity, but substitution with OH in the R_3 position of compound **9** correlates with good activity.

The CoMSIA H-bond acceptor contour plot is shown in Fig. 5d. The magenta areas indicate regions where the H-bond acceptor group increases activity, whereas the cyan contours indicate regions where the H-bond acceptor group decreases activity. A large magenta region flanks ring A. This result is supported by the fact that compound **7** has poor activity. There is hydrogen in the R_2 and R_3 positions, which are in the magenta region. Moreover, the different activity values of compounds **4** and **5** can be explained, even though they have similar structures. Compound **4** has a lower activity than compound **5** as a result of the H-bond acceptor, as shown in the magenta region.

It can be seen that CoMFA contour plots (Fig. 4) correlate with the CoMSIA contour plots (Fig. 5). The CoMSIA results confirm the CoMFA results.

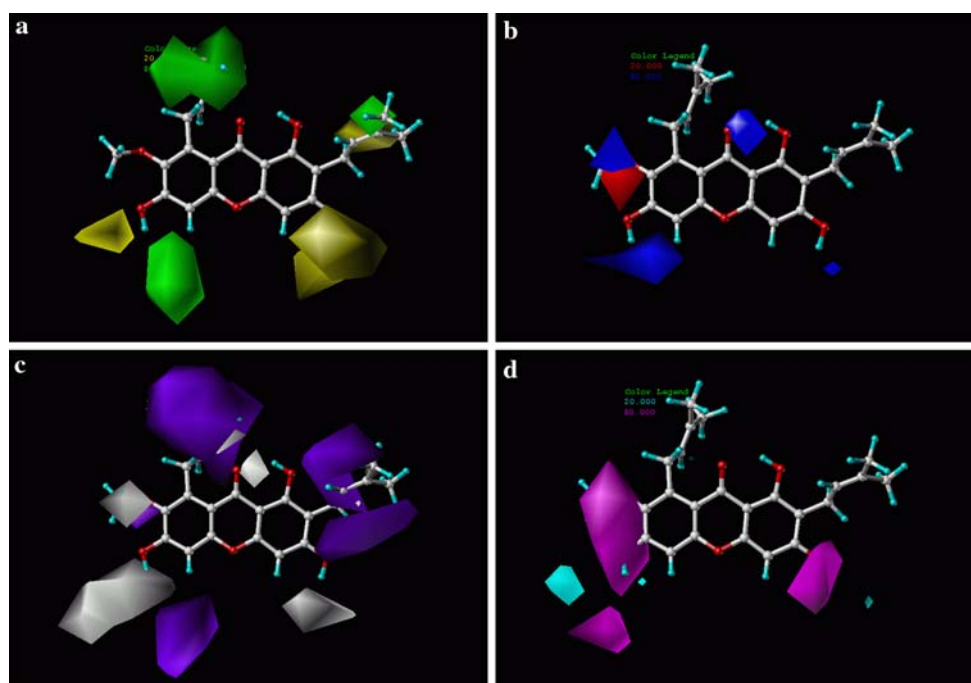


Fig. 5 The four contour maps of CoMSIA ($SD \times \text{coeff}$) model **a** The steric property; *green areas* indicate regions where bulky groups increase activity; *yellow areas* indicate regions where bulky groups decrease activity. **b** The electrostatic property; *blue areas* indicate regions where positive groups increase activity; *red areas* indicate regions where negative charges increase activity. **c** The hydrophobic

property; *purple areas* indicate regions where hydrophobic groups increase activity; *white areas* indicate regions where hydrophilic groups increase activity. **d** The H-bond acceptor property; *magenta areas* indicate regions where H-bond acceptor groups increase activity; *cyan areas* indicate regions where H-bond acceptor groups decrease activity

Conclusion

The CoMFA and CoMSIA analyses were successful in determining the structural requirements of xanthone derivatives against the KB cell line. Both of these analyses give good statistical results in terms of r^2_{cv} and r^2 values. The CoMFA contour maps reveal a significant correlation of the steric and electrostatic properties with the biological activity. In addition, the CoMSIA results include the effect of hydrophobicity and H-acceptors around the binding pocket. The information obtained from the 3D-QSAR results provides helpful guidelines when designing and predicting the affinity of novel xanthone compounds with enhanced activities prior to synthesis.

Methods

Biological data

All synthesized xanthenes [30] were tested for cytotoxic activity against the human KB cancer cell line using the colorimetric method as described by Skehan et al. [31]; the structures and activities are shown in Tables 3 and 4, respectively. The half maximal inhibitory concentration (IC_{50}) values are converted to the negative logarithm of the

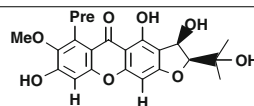
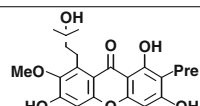
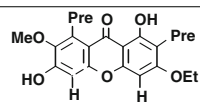
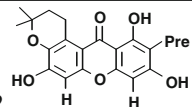
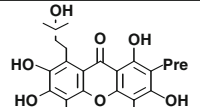
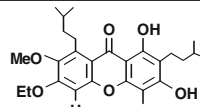
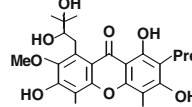
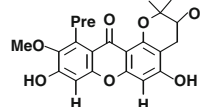
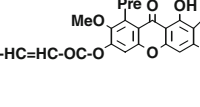
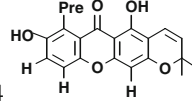
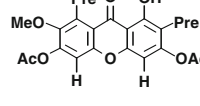
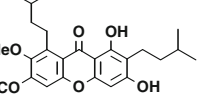
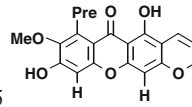
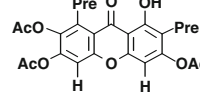
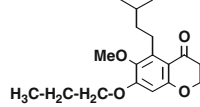
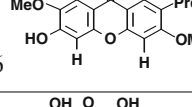
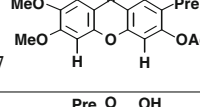
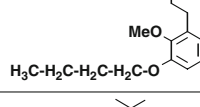
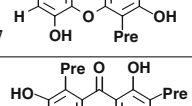
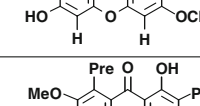
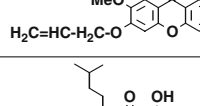
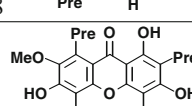
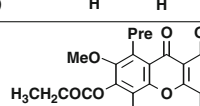
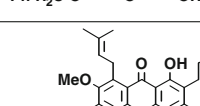
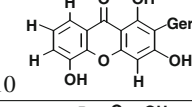
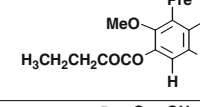
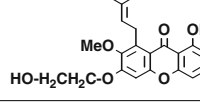
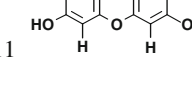
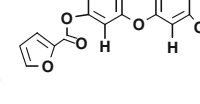
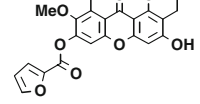
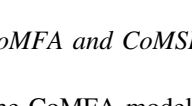
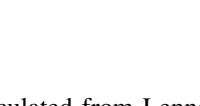
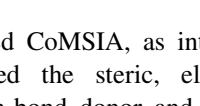
IC_{50} , which is used as the dependent variable in the CoMFA and CoMSIA analyses. Table 4 shows xanthone derivatives that are divided into two sets, consisting of 22 training compounds and 11 tested compounds. The test set is necessary to evaluate the model, so it is selected from a range of xanthone activities. For the test set, three chiral compounds are used in the first selection, and the remaining eight compounds are randomly selected from all compounds.

Molecular 3-D structure building and alignment

The structures of the xanthone derivatives were built using SYBYL 7.0 molecular modeling software [32]. Structural energy minimizations were performed using the PM3 semiempirical molecular orbital method, implemented in the GAUSSIAN 03 program [33]. The Gasteiger charge was used in electrostatic calculations.

The 3D-QSAR methods are ligand-based QSAR techniques. In this study, the most crucial element of the CoMFA and CoMSIA studies is the alignment process. The 3-D structures to be analyzed are aligned on a common structure, as shown in Fig. 1. Compound 9 is selected as template molecule because its activity is greatest. All of the structures of xanthone derivatives are aligned in a 3-D lattice by fitting, matching the atom and superimposing the alignment modules in SYBYL 7.0.

Table 3 Structure of xanthone derivatives against the human KB cancer cell line

Compounds	Compounds	Compounds
 1	 12	 23
 2	 13	 24
 3	 14	 25
 4	 15	 26
 5	 16	 27
 6	 17	 28
 7	 18	 29
 8	 19	 30
 9	 20	 31
 10	 21	 32
 11	 22	 33

CoMFA and CoMSIA studies

The CoMFA models were calculated from Lennard–Jones and Coulombic potential equations, which were characterized as steric and electrostatic fields, respectively. The

reinforced CoMSIA, as introduced by Klebe et al. [34], considered the steric, electrostatic, hydrophobic, and hydrogen-bond donor and acceptor terms. Both CoMFA and CoMSIA were evaluated as 3-D cubic lattices, with a 2-Å grid spacing. The grid points were generated around

Table 4 IC₅₀ values (μg/ml) for cytotoxic activities against the human KB cancer cell line of xanthone derivatives. Compounds **1–14** and **15–33** were taken from [14] and [30], respectively

Number	Compounds	IC ₅₀	–log IC ₅₀
1	Mangostenone C ^a	2.8	5.55
2	Mangostenone D	9.79	5.01
3	Mangostenone E ^a	19.96	4.70
4	Demethylcalabaxanthone ^a	10.9	4.96
5	1,6-Dihydroxy-7-methoxy-8-(3-methylbut-2-enyl)6',6'-dimethylpyranon(2',3':3,2)xanthone	3.72	5.43
6	β-Mangostin	2.5	5.60
7	Gartanin	15.63	4.81
8	Garcinone E	2.67	5.57
9	α-Mangostin	2.08	5.68
10	Mangostinone	12.79	4.89
11	γ-Mangostin	4.69	5.33
12	Garcinone D ^a	3.56	5.45
13	Garcinone C	7.48	5.13
14	11-Hydroxy-1-isomangostin ^a	13.14	4.88
15	3,6-Di- <i>O</i> -acetylmangostin ^a	2.12	5.67
16	3,6,7-Tri- <i>O</i> -acetylmangostin	19.65	4.71
17	3- <i>O</i> -Acetyl-6- <i>O</i> -methylmangostin	6.61	5.18
18	3- <i>O</i> -Benzylmangostin	7.16	5.15
19	6- <i>O</i> -Benzoylmangostin	9.88	5.01
20	3,6-Di- <i>O</i> -propanoylmangostin ^a	7.06	5.15
21	3,6-Di- <i>O</i> -butanoylmangostin	11.0	4.96
22	3,6-Di- <i>O</i> -furanoylmangostin ^a	5.47	5.26
23	3- <i>O</i> -Ethylmangostin	11.3	4.95
24	6- <i>O</i> -Ethyltetrahydromangostin ^a	15.68	4.80
25	6- <i>O</i> -Cinnamoylmangostin	11.25	4.95
26	6- <i>O</i> -Methyltetrahydromangostin	5.17	5.29
27	6- <i>O</i> -Propyltetrahydromangostin ^a	4.63	5.33
28	6- <i>O</i> -Butyltetrahydromangostin	9.02	5.04
29	6- <i>O</i> -Allyltetrahydromangostin	5.57	5.25
30	6- <i>O</i> -Benzyltetrahydromangostin	9.15	5.04
31	6- <i>O</i> -(4-Bromobutyl)mangostin ^a	18.96	4.72
32	6- <i>O</i> -(2-Hydroxyethyl)mangostin	4.96	5.30
33	6- <i>O</i> -Furanoylmangostin	8.93	5.05

^a Test set

the aligned compounds based on the molecular volume of the structure. The grid extended 4 Å in all directions. Molecular interactions were calculated between aligned molecules and three different probe atoms (*sp*³ carbon and hydrogen atoms with +1 charge and an *sp*³ oxygen atom with –1 charge), with superimposition giving the best statistical value of *r*². The maximum cut-offs of the electrostatic and steric energies in the CoMFA model were set as the default values, 30 kcal/mol. The CoMSIA models

were calculated using the C_{sp}³ (+1) probe atom. The matching atom alignment method was selected for the CoMSIA model based on the best statistical value of *r*². The 3D-QSAR models were derived by the partial least squares (PLS) method [34], implemented in SYBYL 7.0. Crossvalidation was used to examine the predictivity of the derived model. The predictive (*r*_{cv}²) ability is defined as

$$r_{cv}^2 = 1 - \frac{\sum_{i=1}^n (y_{i,calculate} - y_{i,experiment})^2}{\sum_{i=1}^n (y_{i,experiment} - y_{i,mean})^2} = 1 - \frac{PRESS}{SSY} \quad (1)$$

and the uncertainty of the prediction (*S*_{press}) is defined as

$$S_{press} = \sqrt{\frac{PRESS}{n - k - 1}} \quad (2)$$

where *k* is the number of variables in the model and *n* is the number of compounds used in the study. The statistical significance of the model is measured by the *F* value:

$$F = \frac{n - k - 1}{k} \frac{\sum_{i=1}^n (y_{i,calculate} - y_{i,mean})^2}{\sum_{i=1}^n (y_{i,experiment} - y_{i,calculate})^2} \quad (3)$$

Acknowledgments This work is supported by the Thailand Research Fund, the Postgraduate Education and Research Program in Chemistry (PERCH) and in Petroleum and Petrochemical Technology (PPT), and a research team strengthening grant from The National Centre for Genetic Engineering and Biotechnology (BIOTEC). Phornphimon Maitarad is grateful to TGIST for a scholarship and the Graduate school of KU for scholarships and to Ben Parslew for English editing. We would like also to thank the High Performance Computing Center of the National Electronics and Computer Technology Center (NECTEC), the Laboratory for Computational and Applied Chemistry (LCAC), and the computing center of KU for research facilities.

References

1. Pravda (2006) Soon cancer to be treated with protons. <http://english.pravda.ru/news/science/22-08-2006/84027-proton-0>. Last accessed 21 June 2008
2. Bilal A (2005) Treating cancer with stem cells. Medical Engineer website (accessed at <http://www.medicalengineer.co.uk/>)
3. Scripture CD, Figg WD (2006) Nat Rev Cancer 6:546
4. Doddareddy MR, Cho YS, Koh HY, Pae AN (2004) Bioorg Med Chem 12:3977
5. Bhongade BA, Gadad AK (2004) Bioorg Med Chem 12:2797
6. Keen N, Taylor S (2004) Nat Rev Cancer 4:927
7. Faivre S, Kroemer G, Raymond E (2006) Nat Rev Drug Discov 5:671
8. Suksamrarn S, Komutiban O, Ratananukul P, Chimnoi N, Lartpornmatulee N, Suksamrarn A (2006) Chem Pharm Bull 54:301
9. Matsumoto K, Akao Y, Kobayashi E, Ohguchi K, Ito T, Tanaka T, Iinuma M, Nozawa Y (2003) J Nat Prod 66:1124
10. Matsumoto K, Akao Y, Yi H, Ohguchi K, Ito T, Tanaka T, Kobayashi E, Iinuma M, Nozawa Y (2004) Bioorg Med Chem 12:5799

11. Moongkarndi P, Kosem N, Kaslungka S, Lanratana O, Pongpan N, Neungton N (2004) *J Ethnopharmacol* 90:161
12. Ho CK, Huang YL, Chen CC (2002) *Planta Med* 68:975
13. Pedro M, Cerqueira F, Sousa ME, Nascimento MS, Pinto M (2002) *Bioorg Med Chem* 10:3725
14. Lin CN, Liou SJ, Lee TH, Chang YC, Won SJ (1996) *J Pharm Pharmacol* 48:539
15. Liou SS, Shich WL, Cheng TH, Won SJ, Lin CN (1993) *J Pharm Pharmacol* 45:791
16. Sultanbawa MUS (1980) *Tetrahedron* 36:1465
17. Suksamrarn S, Suwannapoch N, Phakhodee W, Thanuhiranlert J, Ratananukul P, Chimnoi N, Suksamrarn A (2003) *Chem Pharm Bull* 51:857
18. Peres V, Nagem TJ (1997) *Phytochemistry* 44:191
19. Bennett GJ, Lee HH (1989) *Phytochemistry* 28:967
20. Mandal S, Das PC, Joshi PC (1992) *J Indian Chem Soc* 69:611
21. Pinto MMM, Sousa ME, Nascimento MSJ (2005) *Curr Med Chem* 12:2517
22. Cramer RD, Patterson DEIII, Bunce JD (1988) *J Am Chem Soc* 110:5959
23. Klebe G, Abraham U, Mietzner T (1994) *J Med Chem* 37:4130
24. Depriest SA, Mayer D, Naylor CB, Marshall GR (1993) *J Am Chem Soc* 115:5372
25. Hannongbua S, Lawtrakul L, Sottriffer CA, Rode BM (1996) *Quant Struct Act Relat* 15:389
26. Boström J, Böhm M, Gundertofte K, Klebe G (2003) *J Chem Inf Comput Sci* 43:1020
27. Kubinyi H (1993) *QSAR: Hansch analysis and related approaches*. Wiley-VCH, Weinheim
28. Hansch C, Leo A (1995) *Exploring QSAR fundamentals and applications in chemistry and biology*. American Chemical Society, Washington, DC
29. Böhm M, Stürzebecher J, Klebe G (1999) *J Med Chem* 42:458
30. Suksamrarn S, Sudta P, Kunchanawatta S, Ratananukul P, Suksamrarn A (2007) Thai patent application, No. 0701003620, 27 June 2007, p 36
31. Skehan P, Storeng R, Scudiero D, Monks A, McMahon J, Vistica D, Warren JT, Bokesch H, Kenny S, Boyd MR (1990) *J Natl Cancer Inst* 82:1107
32. Tripos Associates (2008) SYBYL 7.0 molecular modelling software. Tripos Associates, Inc., St. Louis, MO
33. Frisch MJ, Trucks GW, Schlegel HB, Scuseria, GE, Robb MA, Cheeseman JR, Montgomery Jr. JA, Vreven T, Kudin KN, Burant JC, Millam JM, Iyengar SS, Tomasi J, Barone V, Mennucci B, Cossi M, Scalmani G, Rega N, Petersson GA, Nakatsuji H, Hada M, Ehara M, Toyota K, Fukuda R, Hasegawa J, Ishida M, Nakajima T, Honda Y, Kitao O, Nakai H, Klene M, Li X, Knox JE, Hratchian HP, Cross JB, Bakken V, Adamo C, Jaramillo J, Gomperts R, Stratmann RE, Yazyev O, Austin AJ, Cammi R, Pomelli C, Ochterski JW, Ayala PY, Morokuma K, Voth GA, Salvador P, Dannenberg JJ, Zakrzewski VG, Dapprich S, Daniels AD, Strain MC, Farkas O, Malick DK, Rabuck AD, Raghavachari K, Foresman JB, Ortiz JV, Cui Q, Baboul AG, Clifford S, Cioslowski J, Stefanov BB, Liu G, Liashenko A, Piskorz P, Komaromi I, Martin RL, Fox DJ, Keith T, Al-Laham MA, Peng CY, Nanayakkara A, Challacombe M, Gill PMW, Johnson B, Chen W, Wong MW, Gonzalez C, Pople JA (2004) *Gaussian 03*, revision B.04. Gaussian, Inc., Wallingford, CT
34. Wold S, Albano C, Dunn J, Edlund U, Esbensen K, Geladi P, Hellberg S, Johansson E, Lindberg W, Sjostrom M (1987) *Multivariate data analysis in chemistry*. In: Kowalski B (ed) *Chemometrics: mathematics and statistics in chemistry*. Reidel, Dordrecht